Journal of Constructional Steel Research 76 (2012) 54–67

Contents lists available at SciVerse ScienceDirect

Journal of Constructional Steel Research

Compressive behavior of dual-gusset-plate connections for buckling-restrained braced frames

Chung-Che Chou [a,b,*], Gin-Show Liou [c], Jiun-Chi Yu [c]

[a] Department of Civil Engineering, National Taiwan University, Taipei, Taiwan
[b] National Center for Research on Earthquake Engineering, Taipei, Taiwan
[c] Department of Civil Engineering, National Chiao Tung University, Hsinchu, Taiwan

ARTICLE INFO

Article history:
Received 9 July 2011
Accepted 7 March 2012
Available online 26 April 2012

Keywords:
Dual-gusset-plate connection
Buckling-restrained braced frame
Ultimate compression load
Tests
Finite element analysis

ABSTRACT

This work conducts compression tests and finite element analyses for steel dual-gusset-plate connections used for buckling-restrained braced frames (BRBFs). Compared to a single-gusset-plate connection, dual gusset plates sandwiching a BRB core reduce gusset plate size, eliminate the need for splice plates, and enhance connection stability under compression. The experimental program investigated ultimate compression load by testing ten large dual-gusset-plate connections. Out-of-plane deformation of the gusset plate in the test resembled that of a buckled gusset plate with low bending rigidity provided by the BRB end. The general-purpose nonlinear finite element analysis program ABAQUS was applied for correlation analysis. A parametric study of the dual-gusset-plate connection was performed to study the effects of plate size, presence of centerline stiffeners, and beam and column boundaries on ultimate compression load. The ultimate compression load of the dual-gusset-plate connection could not be predicted based on the AISC-LRFD approach due to beam flange out-of-plane deformation. The ultimate compression load of the dual-gusset-plate connection was reasonably predicted using a column strip length from the Whitmore section to the workpoint of the beam and column centerlines and a buckling coefficient of $K=2$.

1. Introduction

Buckling-restrained braced frames (BRBFs) for lateral load resistance have been increasingly used in recent years [1–5]. The BRBF differs from a steel concentrically braced frame (CBF) because a buckling-restrained brace (BRB) yields in both tension and compression without global buckling. Since the restraining member provides continuous lateral support for the BRB core, high-mode buckling in the core maintains stable energy dissipation under compression [4]. For a BRB with a single core, a single gusset plate, commonly used in CBFs, is adopted in BRBFs to connect a BRB to the beam and column (Fig. 1(a)). Many splice plates and bolts are used to connect a single gusset plate and a BRB core. During a severe earthquake, braces in CBFs are subjected to large axial deformations in cyclic tension and compression into the post-buckling range. For a brace buckling out of plane with single plate gussets, weak-axis bending in the gusset is induced by member end rotations. Satisfactory performance of a brace can be ensured by allowing the gusset plate to develop restraint-free plastic rotations, *i.e.* buckling [6]. Conversely, no gusset plate buckling is allowed in a BRBF during a severe earthquake, ensuring stable energy dissipation in the BRB. The AISC seismic design provisions [6] require consideration of gusset plate instability because recent BRBF tests by Chou and Liu [5], Aiken et al. [7], Tsai et al. [8], and Chou and Chen [9] demonstrated out-of-plane gusset plate buckling before a BRB reached ultimate compression load.

The compressive behavior of gusset plate connections in a CBF has received limited attention [10]. Thornton [11] proposed that buckling load of a gusset plate ($P_{cr,Th}$) can be considered as the compressive strength of a fixed–fixed column strip below the Whitmore effective width [12], b_e (Fig. 1(b)). The length of the column strip, L_c, is the maximum of L_1, L_2, and L_3; the buckling coefficient, K, is 0.65. A column buckling equation combined with the Whitmore sectional area is adopted to estimate ultimate compression load of a gusset plate. Gross and Cheok [13], however, used the average of lengths L_1, L_2, and L_3 and K of 0.5 to estimate the buckling load of a gusset plate ($P_{cr,GC}$). When the end of a brace moves out of plane, a conservative value of 1.2 or 2 for K in the column buckling equation was recommended by Astaneh-Asl [14] and Tsai et al. [8], respectively. Thornton's design concept, adopted in the AISC-LRFD specification and design examples [15,16], is used to estimate ultimate load of a gusset plate under compression, $P_{cr,AL}$:

$$P_{cr,AL} = (0.658)^{\lambda_c^2} b_e t F_y, \quad \lambda_c \le 1.5$$
$$P_{cr,AL} = \left(\frac{0.877}{\lambda_c^2}\right) b_e t F_y, \quad \lambda_c > 1.5 \tag{1}$$

* Corresponding author at: Dep. of Civil Engineering, National Taiwan Univ., Taipei, Taiwan. Tel.: +886 2 3366 4349; fax: +886 2 2739 6752.
E-mail address: cechou@ntu.edu.tw (C.-C. Chou).

0143-974X/$ – see front matter © 2012 Elsevier Ltd. All rights reserved.
doi:10.1016/j.jcsr.2012.03.003

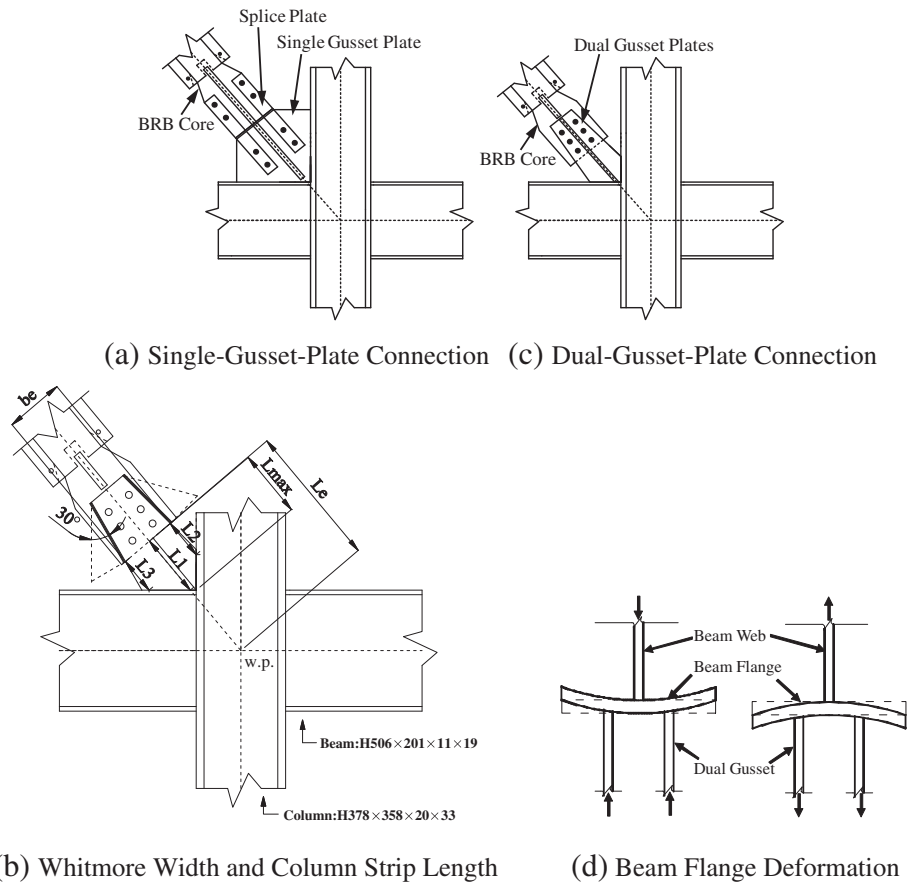

Fig. 1. Single and dual gusset plate connections.

where $\lambda_c = \frac{KL_c}{\pi r}\sqrt{\frac{F_y}{E}}$, t is the plate thickness, r is the radius of gyration, E is the steel elastic modulus, and F_y is the steel yield strength. The length of the column strip, L_c, is either the average of lengths, L_1, L_2, and L_3, or L_1 (Fig. 1(b)). The K value, which is from Page IIC-39 of AISC design examples [16], is 0.5 for a gusset plate supported on four edges and 1.2 for a gusset plate supported on two edges.

Although gusset plate connections are widely used in BRBFs, the research, both experimental and analytical, is insufficient to provide a complete design guideline. Specifically, gusset plates in a BRBF need to carry ultimate compression load of a BRB without buckling, which differs from those in a CBF. Therefore, this work investigates the compressive behavior and ultimate load of gusset connections in a BRBF. A dual-gusset-plate configuration (Fig. 1(c)), connecting the BRB core via two identical plates, is proposed in this study. The objective is to eliminate the need for splice plates, minimize the number of bolts, and reduce gusset size. Moreover, two gusset plates placed outside a BRB core are more stable than a single gusset plate under compression due to the greater moment of inertia for the same gusset thickness. The experimental program consists of testing 10 large gusset specimens; test parameters are plate thickness, plate size, and presence of centerline stiffeners. Test results are then compared with predictions using the current AISC code and those in previous research. A general-purpose nonlinear finite element analysis program ABAQUS [17] is used to perform a correlation study. A parametric study using finite element analysis is then performed to investigate the effects of gusset plate thickness, plate size, presence of centerline stiffeners, and beam and column boundaries on the ultimate load of a dual-gusset-plate connection.

The dual-gusset-plate connection as the single-gusset-plate connection can develop plastic rotation after buckling, and is, therefore, applicable to ductile CBFs. In this case, the gussets should be designed to deform to accommodate brace buckling after successfully resist the brace buckling compression force without buckling. However, out-of-plane buckling of gusset plates requires high ductility demand on successive bending behavior, which is beyond the scope of the test in this study.

2. Buckling-restrained braced frame

2.1. BRBF design

Fig. 2 shows the plan and elevation of the prototype building, which was assumed to be located on stiff soil in Los Angeles, California. Two one-bay BRBFs providing lateral load resistance in the north–south direction were considered in this study. Design of the prototype building is to find appropriate sizes of a gusset connection and BRB for testing. The design dead loads were 5.28 kPa (110 psf) and 4.32 kPa (90 psf) for floors and the roof, respectively, while the live loads for both the floors and the roof were 2.39 kPa (50 psf). Effective seismic weights for floors and the roof were 3834 kN and 3136 kN, respectively, resulting in a total seismic building weight of 22,306 kN. The design followed the AISC seismic provisions [6] with a force reduction factor, R, of 8, an over-strength factor, Ω_0, of 2.5 and a deflection amplification factor, C_d, of 5. The mapped spectral response accelerations at a short period S_S and one second S_1 were 1.5 g and 0.6 g, respectively. For the building located at site class D, the site coefficients F_a and F_v were 1.0 and 1.5, respectively, leading to design spectral response accelerations at a short period and one second of 1.0 g and 0.6 g, respectively. The structural period, T, and seismic response coefficient, C_s, calculated by IBC [18] were 0.8 s and 0.094, respectively, such that the seismic

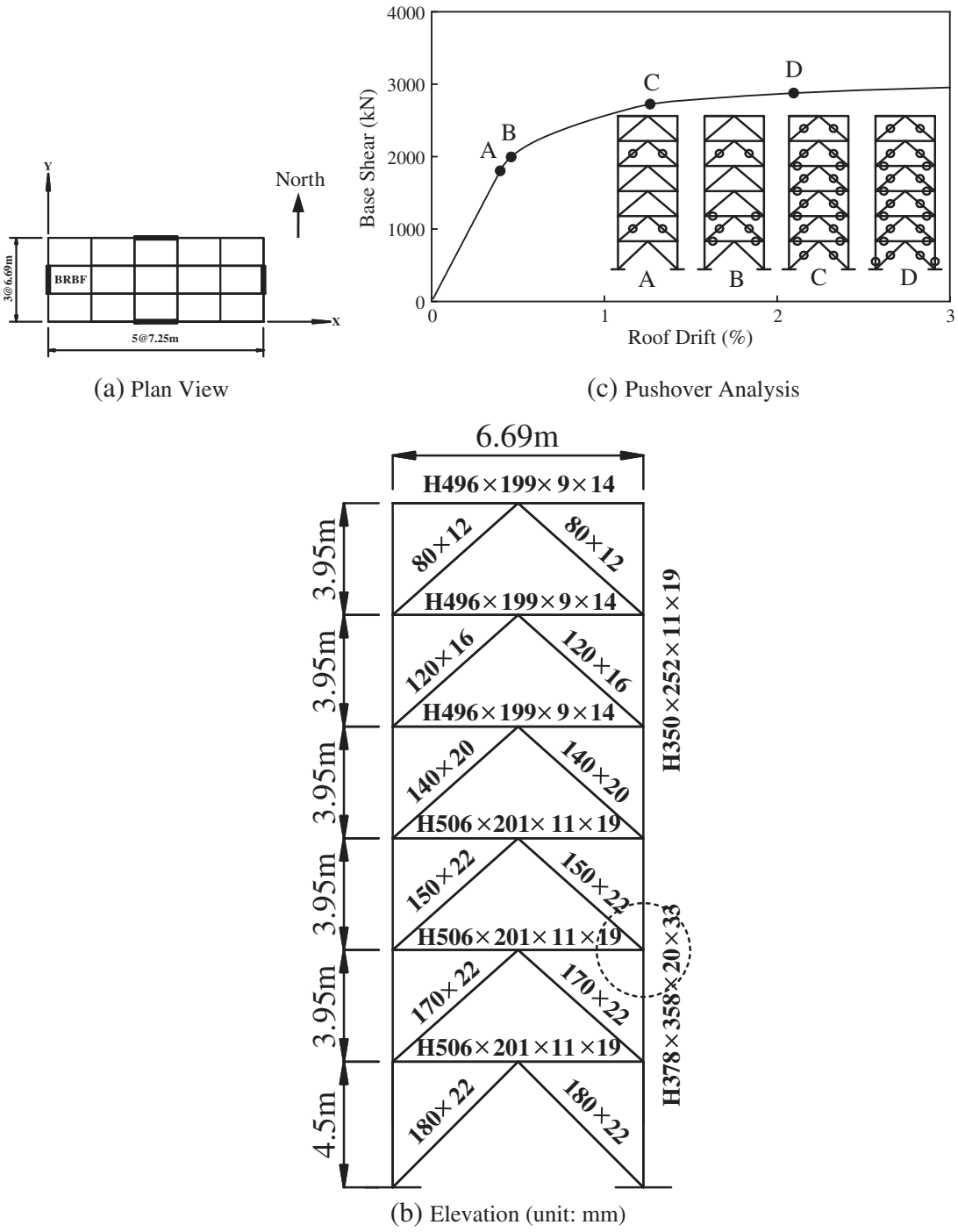

Fig. 2. Prototype frame and pushover analysis.

base shear, V_{des}, for one BRBF was 1049 kN. Fig. 2(b) lists the selected beam, column, and BRB core sizes.

The BRBF was analyzed using the computer program, PISA [19]. The beam, column, and BRB members were modeled using one dimensional steel beam-column elements which consist of two nodes, each with three degrees of freedom: the translations in the x and y-directions and the rotation in the z-direction. A bilinear inelastic model with a strain- hardening ratio of 4% was introduced to model the plastic hinge in the BRB, beam, and column. The strength and stiffness degradation of the flexural hinges were not considered in the numerical model. The panel zone deformation and the P-Delta effects due to gravity loading were not considered in the model. Axial forces due to gravity loads were assigned at each column node. Fixed end moments and shear forces caused by gravity loads on the beams were applied at both ends of elements representing the beam members. A Rayleigh type damping of 5% of critical was assigned for the first mode and the third mode.

Monotonic pushover analysis for the BRBF was conducted to obtain the force-deformation relationship. The IBC load pattern [18] with increasing amplitude was applied to push the BRBF. Fig. 2(c) shows the relationship between base shear and roof drift of the BRBF. First-yield strength, V_{y1}, of the BRBF was 1780 kN ($=1.7V_{des}$) when BRBs in the second and fifth floors yielded at a roof drift of 0.4% (step A). The base shear reached 2002 kN ($=1.9V_{des}$) and

2875 kN ($=2.7V_{des}$) corresponding to yielding in the beam and column base, respectively (Steps B and D). Overstrength calculated using the ideal yield force of 2750 kN divided by the design force of 1049 kN was 2.6, which is close to 2.5, as in AISC seismic provisions [6].

The sandwiched BRB in this work has a steel core and two identical restraining members formed by welding a steel channel to a face plate and then filling the cavity with concrete or mortar (Fig. 3). Unlike conventional BRBs that have a steel core inserted into a restraining member, sandwiching a core plate between a pair of restraining members using high-strength A490 bolts expedites the assembly process. A small gap between the steel core and buckling-restraining member is utilized to minimize axial force transfer from the steel core to the buckling-restraining member. Only the steel core is designed to provide axial load to the BRB. The maximum tension force, $T_{\max}$, and maximum compression force, C_{max}, of the BRB are

$$T_{\max} = \Omega_h \Omega A_y F_y \tag{2}$$

$$C_{\max} = \beta \Omega_h \Omega A_y F_y \tag{3}$$

where Ω_h is the strain hardening factor, Ω is the material overstrength factor, and A_y is the cross-sectional area of the steel core. According to component and frame test results [4,5], the compression strength adjustment factor, β, was 1.15.

The BRB core positioned on the third floor was a plate 150 mm wide by 22 mm thick, made of ASTM A572 Gr. 50 steel. Maximum tension force, $T_{\max}$, and maximum compression force, C_{max}, were 1566 kN and 1811 kN, respectively. The AISC Seismic Provisions [6] require that axial capacity of a gusset plate exceeds the ultimate compression load of a BRB to ensure stable energy dissipation. To investigate the compression capacity of a dual-gusset-plate connection, a BRB with yield capacity of 2200 kN, exceeding 1811 kN, was used. Thus, a gusset plate connection with an ultimate compression load smaller than the BRB yield capacity (2200 kN) could be used in the test setup (Fig. 4(a)).

2.2. Gusset specimen

In total, 10 dual-gusset-plate connections were fabricated and tested. Test parameters were gusset plate thickness, plate size, centerline stiffener length, and connection type between the dual gusset plates and BRB. Thin plates, 8 mm and 12 mm, made of ASTM A572 Gr. 50 steel, were used to fabricate the gusset plates. Fig. 5 and Table 1 show specimen dimensions. Each gusset specimen had two identical plates bolted and welded to the web of a T device at the BRB end (Fig. 4(b)). The T device was composed of a flange plate and web plate, which had the same thickness as the BRB core (22 mm). The T-device was a transition device for test not for application purposes. Using the T-device to connect a dual-gusset-plate and a BRB protected the BRB core from damage while the dual-gusset-plate buckled. Since the BRB core and the web plate of the T device existed in the co-plane, the force transfer from the BRB to the gusset was simulated with the T device to the gusset. As long as the installation of the T device was aligned with the BRB core, the T device did not affect the stability of the assembly. Dual gusset plates were groove-welded to the beam and column interfaces; the BRB with the T device was bolted to dual gusset plates. Additional fillet weld was applied to connect the T device and dual gusset plates when the bolt capacity could not resist ultimate load of the BRB (Fig. 4(b)). Specimens 1–5 had 8-mm-thick dual gusset plates. Specimens 1 and 2 were identical, except that their column strip lengths were 266 mm and 197 mm, respectively. Specimens 3–5 were identical to Specimen 1, except that the lengths of their centerline stiffeners welded to each gusset plate were 90, 548, and 314 mm, respectively. Specimens 6–10 had 12-mm-thick dual gusset plates. Specimens 6 and 7 were identical, except that their column strip lengths were 266 mm and 197 mm, respectively. Specimens 8 and 9 were identical to Specimen 6, except that their centerline stiffener lengths were 548 and 314 mm, respectively. Specimen 10 was

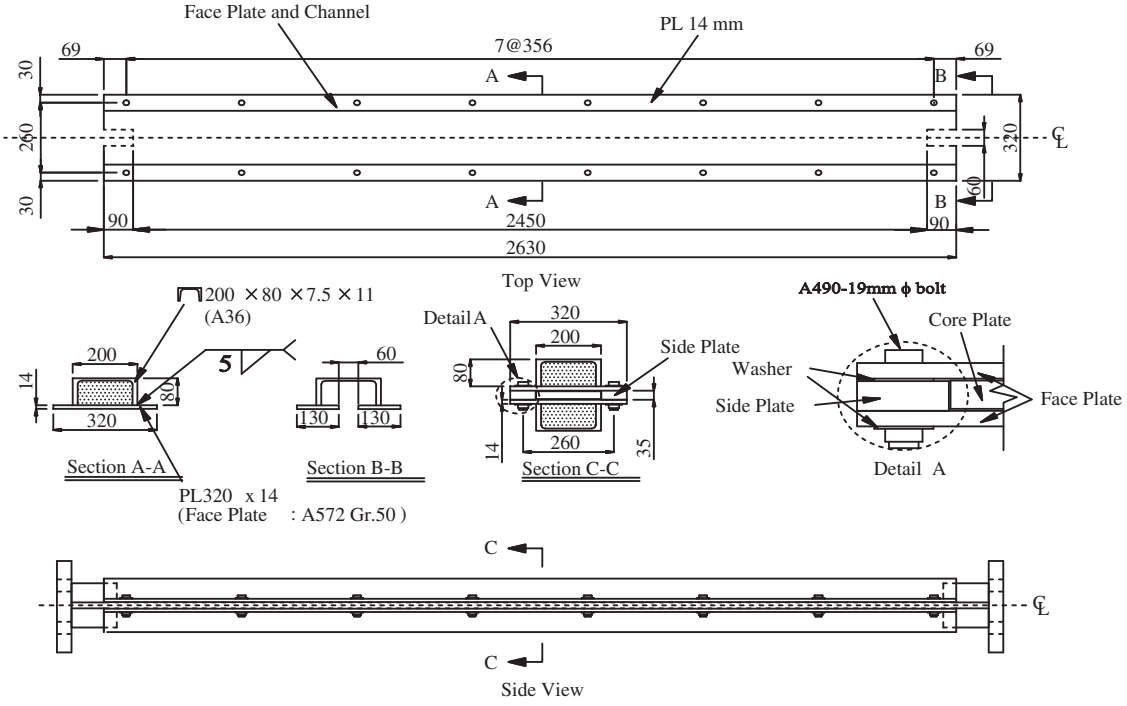

Fig. 3. BRB details (unit: mm).

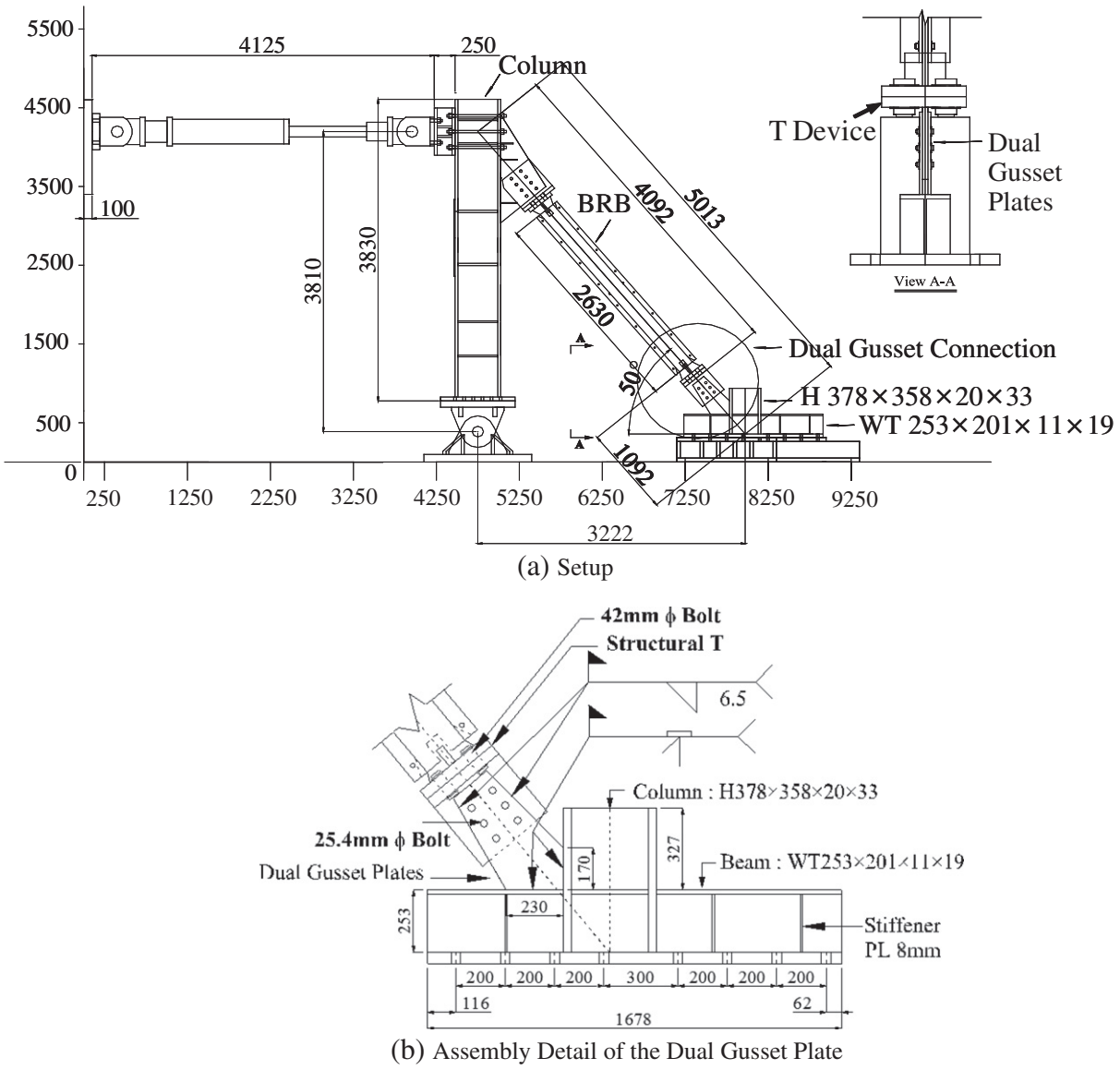

Fig. 4. Test setup and dual gusset assembly (unit: mm).

identical to Specimen 9, except that its bolted joint was replaced by a fillet welded joint. Table 1(b) lists predicted compression loads based on previous studies [8,11,13–16].

3. Experimental program

3.1. Test setup and instrumentation

Fig. 4(a) shows the test setup, which had one column pin-supported to the laboratory's strong floor and attached to two 1000-kN hydraulic actuators. The H378 × 358 × 20 × 33 and WT 253 × 201 × 11 × 19 sections in the setup were used to simulate the column and beam on the third floor of the prototype. The BRB was positioned at θ = 50° with both ends connected by dual gusset plates. The specimen was subjected to a prescribed cyclic displacement history with increasing amplitude until unloading occurred (Table 2). Because the BRB remained elastic and the deformation of dual gussets were small during testing, the testing protocol did not follow cyclic loading protocol specified by AISC (2005). When the gusset plate buckled, the BRB core was inspected and replaced with a new core if it buckled at its end. Linear variable displacement transducers (LVDTs) were used to measure axial displacement and out-of-plane displacement of the gusset plate and BRB. Strain gauges were mounted on each gusset plate to measure strain distribution. Gusset plates were painted such that material yielding was indicated by flaking paint.

3.2. Experimental results

Fig. 6 shows the axial force versus axial displacement relationship of eight specimens. Buckling load of the specimen, $P_{cr,Test}$, was defined as the ultimate compression load before specimen unloading (Table 3). The ultimate compression stress, $F_{cr,Test}$, was calculated by dividing $P_{cr,Test}$ by the Whitmore effective area ($=2b_e t$). Overall plate buckling was a primary failure mode for all specimens; however, local plate buckling, which did not affect load carrying capacity, existed in specimens with centerline stiffeners. No obvious yield lines existed in Specimens 1–3 and 6 before the gusset plate buckled (Fig. 7). Specimen 4 was cyclically loaded up to a 0.05% column drift and then monotonically compressed until gusset plate buckling occurred. When the axial load in Specimen 4 reached 920 kN, yield lines occurred in the Whitmore section and near the column interface. Local plate buckling occurred between the centerline stiffener and gusset

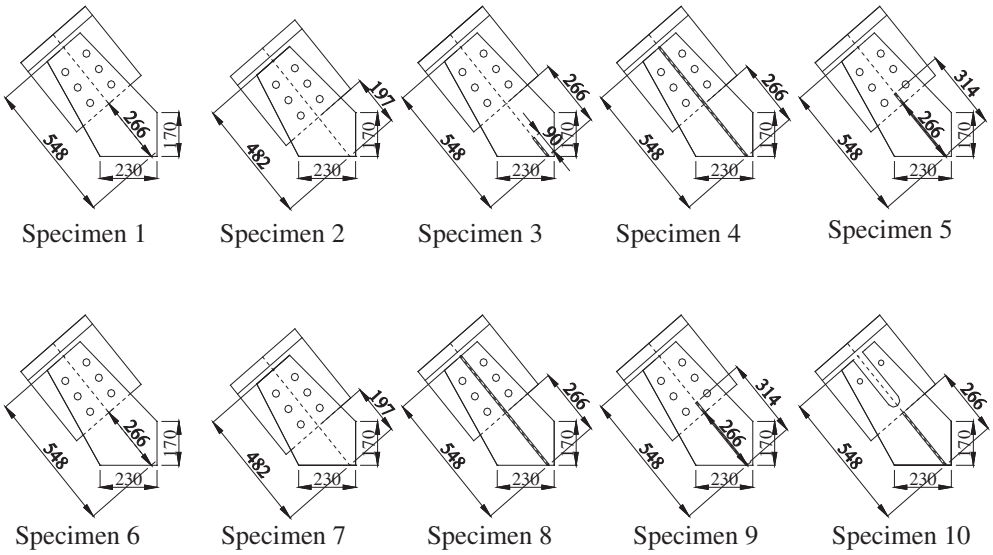

Fig. 5. Specimen dimension (unit: mm).

plate free edge (Fig. 8(a)). When an ultimate load of 1594 kN was reached, dual gusset plates buckled (Fig. 8(b) and (c)). Plate buckling was also observed along the centerline stiffener length (Fig. 8(d)). Similar plate buckling was observed in the dual-gusset-plate connection specimens with centerline stiffeners, all which had $F_{cr,Test}$ values exceeding $0.7F_y$, except for Specimen 10, which had a $F_{cr,Test}$ value of $0.64F_y$ (Table 3).

Fig. 9 shows the out-of-plane deflected shapes of the BRB and gusset plate when ultimate compression load was reached. The deflected shape was normalized by a maximum out-of-plane deformation of a specimen. Typical buckled shapes for dual-gusset-plate connections resembled the buckled shape of a fixed-free column with an inflection point at the BRB end (L11). However, the inflection point of the buckled gusset plate was near the Whitmore section (L17) for Specimens 1 and 3, which had the thinnest and longest gusset plate among all specimens. Fig. 10 shows the out-of-plane deflected shapes of gusset connections only. The deflection increased as the load increased and it did not affect the load-carrying capacity of

Table 1
Specimen dimension and predicted compression load.

(a) Dimension and strength

Specimen	t (mm)	b_e (mm)	L_1 (mm)	Stiffener length (mm)	Stiffener width (mm)	Plate strength	
						F_y (MPa)	F_u (MPa)
1	8	248	266	–	–	444	521
2	8	263	197	–	–	409	518
3	8	248	266	90	–	444	521
4	8	248	266	548	45	444	521
5	8	248	266	314	45	444	521
6	12	248	266	–	–	406	514
7	12	263	197	–	–	442	517
8	12	248	266	548	45	380	474
9	12	248	266	314	45	406	514
10	12	248	266	266	45	406	514

(b) Predicted compression load

Spe.	Thornton ($K=0.5$)		Gross and Cheok ($K=0.65$)		Astaneh-Asl ($K=1.2$)		AISC-LRFD ($K=1.2$)		Tsai et al. ($K=2.0$)	
	L_c (mm)	$P_{cr,\,Th}$ (kN)	L_c (mm)	$P_{cr,\,GC}$ (kN)	L_c (mm)	$P_{cr,\,As}$ (kN)	L_c (mm)	$P_{cr,\,AL}$ (kN)	L_c (mm)	$P_{cr,\,Ts}$ (kN)
1	266	1741	195	1755	281	1683	195	1723	266	1572
2	197	1711	122	1719	212	1680	122	1707	197	1625
3	266	1741	195	1755	281	1683	195	1723	266	1572
4	266	2070	195	2078	281	2037	195	2060	266	1972
5	266	2070	195	2078	281	2037	195	2060	266	1972
6	266	2396	195	2410	281	2340	195	2380	266	2231
7	197	2776	122	2787	212	2735	122	2772	197	2660
8	266	2524	195	2532	281	2491	195	2514	266	2426
9	266	2695	195	2705	281	2658	195	2684	266	2584
10	266	2695	195	2705	281	2658	195	2684	266	2584

Table 2
Loading history.

No. of cycle	2	2	2	2	2	2	2	2	2	2
Actuator Displacement (mm)	±0.5	±1	±2	±4	±6	±8	±10	±12	±14	±16
Drift ratio (%)	0.01	0.03	0.05	0.1	0.16	0.21	0.26	0.31	0.36	0.42

dual gusset plates under cyclic loading until significant overall plate buckling occurred. Except for Specimens 1 and 3, buckling occurred in all specimens when the actuator moved 16 mm. Note that the gusset boundary at the beam-to-column interface, measured by displacement transducer, L13 (Fig. 10(a)), showed out-of-plane deformation under compression because the beam flange had no lateral support. This indicates that when calculating the critical buckling load of a gusset plate, column strip length should be extended from the beam-to-column interface to the workpoint of the beam and column centerlines.

3.2.1. Gusset plate thickness

The maximum load of a specimen was greatly affected by gusset plate thickness. By increasing gusset plate thickness from 8 mm (Specimen 1) to 12 mm (Specimen 6), the ultimate compression load of a specimen was increased 1.6 times (Table 3). The ultimate compression

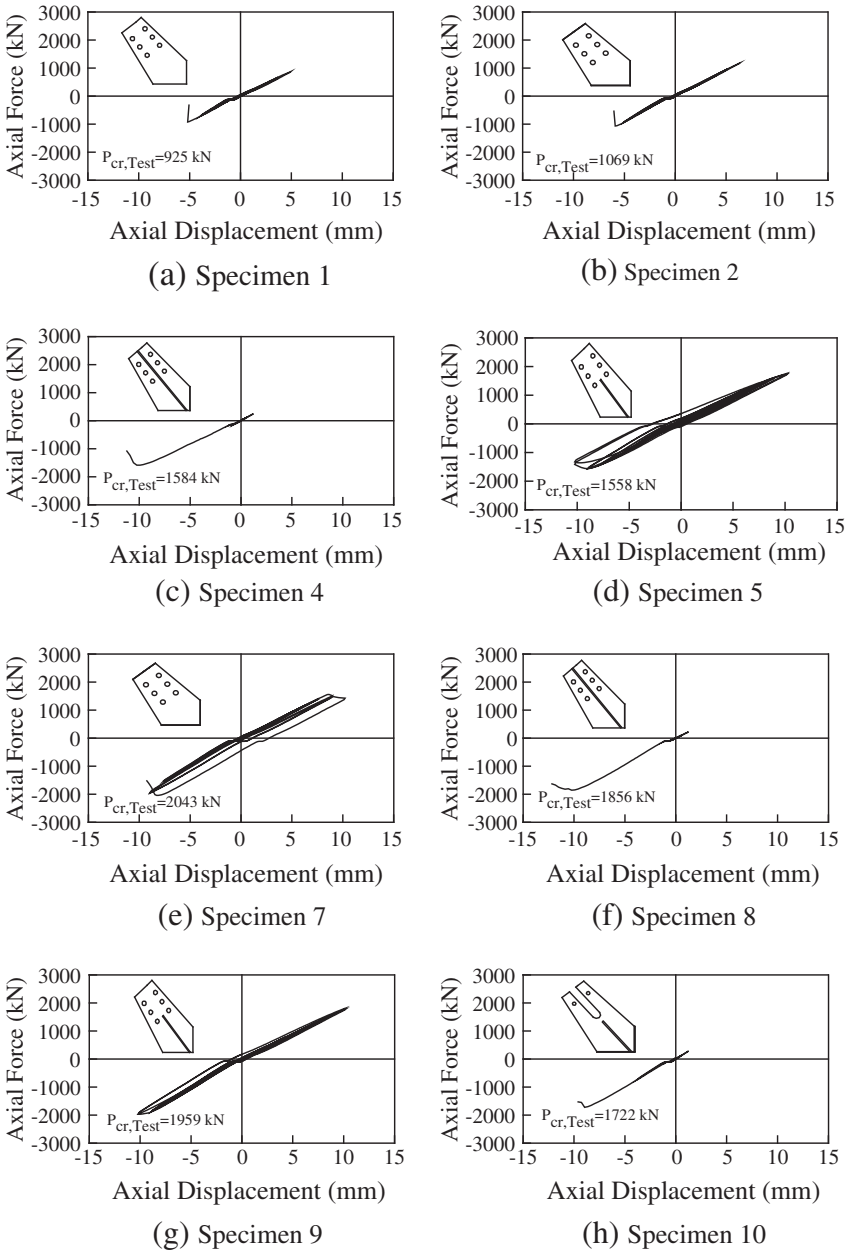

Fig. 6. Axial force versus axial displacement relationship.

Table 3
Ultimate compression load.

Specimen	$P_{cr,Test}$ (kN)	$F_{cr,\ Test}$ (MPa)	$\frac{F_{cr,Test}}{F_y}$	$\frac{P_{cr,Test}}{P_{cr,Th}}$	$\frac{P_{cr,Test}}{P_{cr,GC}}$	$\frac{P_{cr,Test}}{P_{cr,As}}$	$\frac{P_{cr,Test}}{P_{cr,AL}}$	$\frac{P_{cr,Test}}{P_{cr,Ts}}$	$\frac{P_{cr,Test}}{P_{cr,CY}}$	$\frac{P_{cr,Test}}{P_{cr,ABA}}$
1	925	233	0.52	0.53	0.53	0.55	0.53	0.59	0.94	0.92
2	1069	254	0.62	0.62	0.62	0.64	0.62	0.66	0.94	0.93
3	1121	283	0.64	0.64	0.64	0.67	0.64	0.71	1.14	1.07
4	1584	338	0.76	0.76	0.76	0.78	0.76	0.80	1.00	0.88
5	1558	332	0.75	0.75	0.75	0.76	0.75	0.79	0.99	0.92
6	1522	256	0.63	0.63	0.63	0.65	0.63	0.68	0.94	0.96
7	2043	324	0.73	0.74	0.73	0.75	0.73	0.77	1.03	1.07
8	1856	278	0.73	0.74	0.73	0.75	0.73	0.77	0.92	0.94
9	1959	294	0.72	0.73	0.72	0.74	0.73	0.76	0.92	0.88
10	1722	258	0.64	0.64	0.64	0.65	0.64	0.67	0.81	0.88

load of Specimen 7 was approximately two times that of Specimen 2. However, the ultimate compression load caused by increasing gusset plate thickness increased only 1.17 times in Specimens 4 and 8, which had centerline stiffeners. This increase was much smaller than that in specimens without centerline stiffeners.

3.2.2. Column strip length in gusset plate

Fig. 5 shows that two column strip lengths of 197 mm and 266 mm were used for specimens without centerline stiffeners. For an 8-mm-thick gusset plate, ultimate compression load was governed by gusset plate instability in the Whitmore section (Specimen 1). Ultimate compression load increased when column strip length in Specimen 2 decreased, as compared to that in Specimen 1 (Table 3). For a 12-mm-thick gusset plate, the ultimate compression load also increased when column strip length decreased, as seen by comparing Specimen 7 to Specimen 6. This increase was larger in the thick-plate specimen than in the thin-plate specimen.

3.2.3. Centerline stiffeners

Specimens 1–2 and Specimens 6–7 failed due to overall plate buckling. To improve the compression strength of gusset plates, centerline stiffeners welded outside of the dual gusset plates were adopted in the other specimens. Other possible stiffener configurations, namely, free-edge stiffeners, which are welded along the length of gusset plate unsupported edges, can be used to increase ultimate loads of specimens [9]. However, for the compact gusset plates, which fail due to overall plate buckling, centerline stiffeners are more efficient than free-edge stiffeners in stiffening the gusset plate connection [20]. According to the provision provided by CAN/CSA-S6-88-Design of Highway Bridges [21], the a/t ratio is limited to $945/\sqrt{F_y}$ to satisfy the compact section requirement, where a is the length of a long free edge of a gusset plate. The a/t ratios for the thin gusset plate ($t=8$ mm) and thick gusset plate ($t=12$ mm) were 20.5 and 13.6, both less than $945/\sqrt{F_y}(=47)$. Therefore, all specimens in this study were compact gusset plates.

The ultimate compression loads of specimens increased with the use of centerline stiffeners and also increased as the length of centerline stiffeners increased (Table 3). For thin gusset plates, the ultimate compression load for Specimen 4 ($P_{cr,Test}=1584$ kN), which had the longest centerline stiffeners, was 1.7 times that for Specimen 1 ($P_{cr,Test}=925$ kN), which lacked centerline stiffeners. For thick gusset plates, the ultimate compression load for Specimen 8 ($P_{cr,Test}=1856$ kN), which had the longest centerline stiffeners, was 1.2 times that for Specimen 6 ($P_{cr,Test}=1522$ kN), which lacked centerline stiffeners. This finding indicates that adding centerline stiffeners is more efficient in increasing ultimate compression load

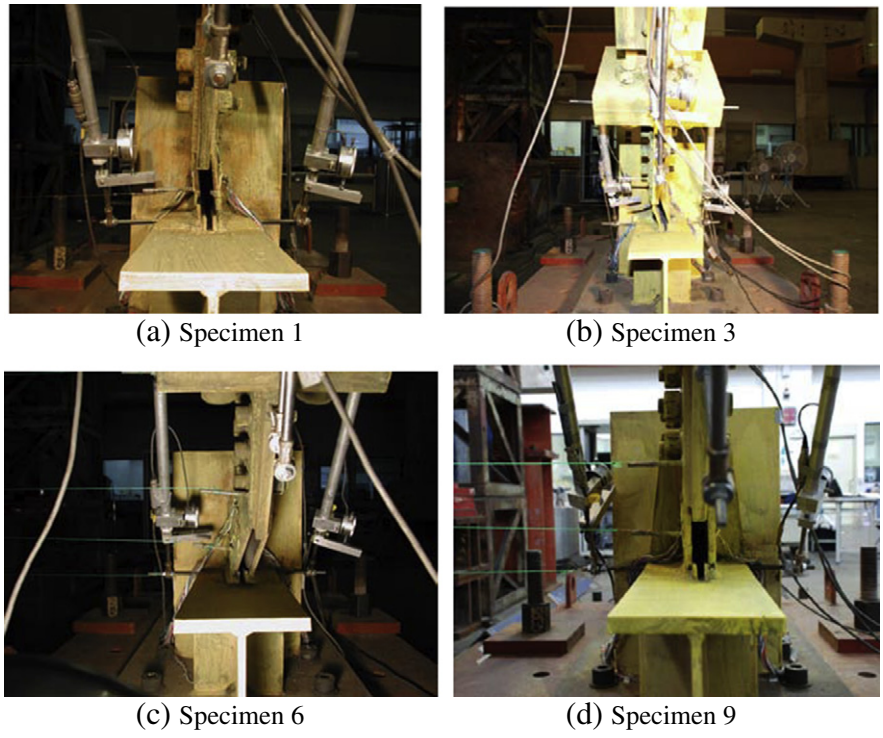

Fig. 7. Overall buckling of dual gusset plates.

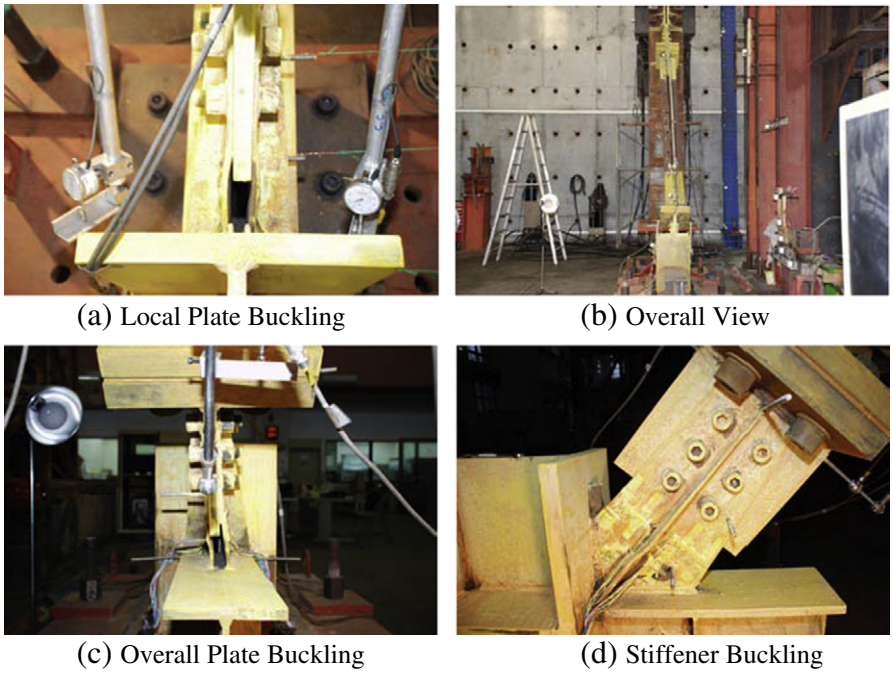

Fig. 8. Observed performance in Specimen 4.

of a thin plate than a thick plate. As long as a centerline stiffener extends beyond the Whitmore section, additional extension only slightly affects the ultimate compression loads of dual-gusset-plate connections (Specimen 4 *versus* Specimen 5).

3.3. Ultimate compression load prediction

Table 3 shows the ratios of ultimate compression load from test, $P_{cr,Test}$, to those predicted based on AISC-LRFD specification ($P_{cr,AL}$), Thornton ($P_{cr,Th}$), Gross and Cheok ($P_{cr,GC}$), Astaneh-Asl ($P_{cr,As}$), and Tsai et al. ($P_{cr,Ts}$). The ultimate compression load formula developed based on the fixed-fixed column strip [11,13] cannot be used to estimate compression loads of gussets with a fixed-free boundary. However, compression loads calculated based on the buckling coefficient, K, of 1.2 ($P_{cr,As}$) and 2 ($P_{cr,Ts}$), as recommended by Astaneh-Asl [14] and Tsai et al. [8], respectively, significantly overestimated gusset plate ultimate load, $P_{cr,Test}$. In considering the effects of an unsupported beam flange during testing, which causes a gusset plate to deform laterally at the beam-to-column interface, the ultimate compression load of a gusset plate ($P_{cr,CY}$) is calculated based on a fixed-free column strip, L_e, measured from the Whitmore section to the workpoint of the beam and column centerlines (Fig. 1(b)), and a K value of 2. Specimens 2 and 7 have a column strip length of $L_e = 527$ mm, and others have $L_e = 596$ mm. The predicted ultimate compression loads, $P_{cr,CY}$, are close to those obtained from tests and their $P_{cr,Test}/P_{cr,CY}$ ratios are in the range of 0.81–1.14 (Table 3). Moreover, for using centerline stiffeners across the Whitmore section, i.e. Specimens 4, 5, 8, and 9, the area and moment of inertia of centerline stiffeners along the Whitmore section of a gusset plate are included in computing compression load in Eq. (1). Table 3 lists compression loads of gussets predicted using the proposed method and other methods. It shows that the proposed method reasonably predicts ultimate compression loads of stiffened gusset connections.

The dual-gusset-plate connection is placed away from the beam web, so the brace load bends the beam flange as shown in Fig. 1(d). A single-gusset-plate connection does not accompany the behavior of beam flange bending because the beam web, gusset, and column web exist in the co-plane. Since the dual-gusset-plate connection has different geometric configuration and structural characteristics compared to the single-gusset-plate connection under a load, the prediction based on previous studies [8,11,13–16] is not close to the test result in this study (Table 3). The error in prediction can be minimized by using the effective length of the strut measured from work point to brace end. When the beam flange is restrained, the strut measured from the beam-to-column interface to brace end per current practice can be used to predict ultimate compression load of the gusset connection.

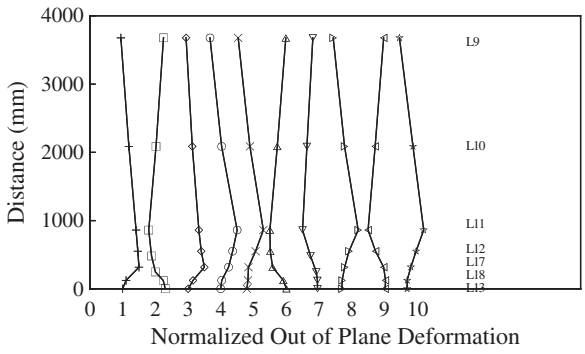

Fig. 9. Normalized out-of-plane deformation under loading $P_{cr,\ Test}$ (along BRB and gusset length).

4. Finite element analysis

4.1. Finite element models

The finite element analysis program ABAQUS [17] was used to investigate the compressive behavior and strength of all specimens. Fig. 11(a) shows an analytical model comprising a beam, column, base plate, and a T device, which was placed between dual gusset plates. No slippage during the test occurred between the dual gusset plates and the T device; thus, a fully-bonded interface between these two parts was used. Material nonlinearity with the von Mises yielding criterion was considered in the models. Yield stress obtained from the coupon test (Table 1(a)) was adopted for each specimen. The elastic modulus of steel was 203 GPa. Eight-node solid elements, C3D8R, with three degrees of freedom at each node were used in the model.

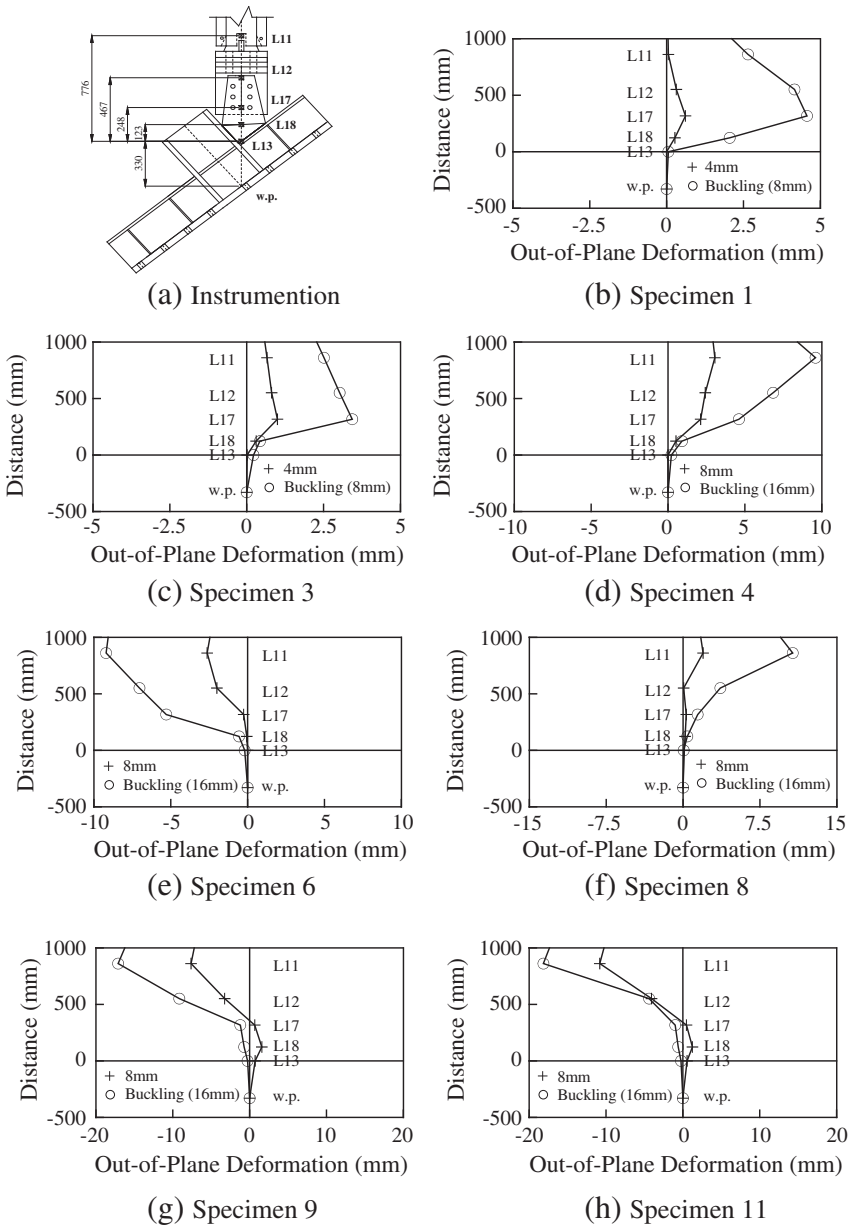

Fig. 10. Gusset out-of-plane deformation.

Axial displacement was applied at the T device to simulate load transfer during the tests. Since the initial imperfection of dual gusset plates was not measured in the tests and its shape was considerably less critical than magnitude based on the previous work [10], the first buckling mode shape (Fig. 11(b)) was adopted as the initial imperfection (1/1000 times gusset length) before analysis.

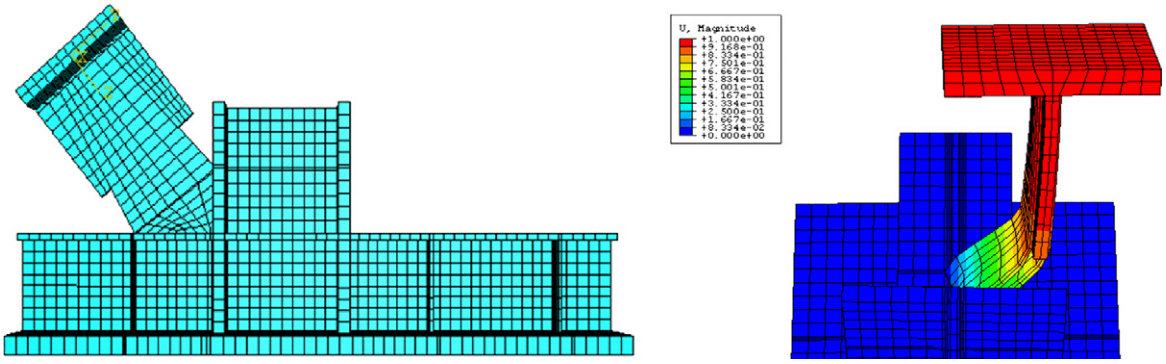

Fig. 11. Finite element model.

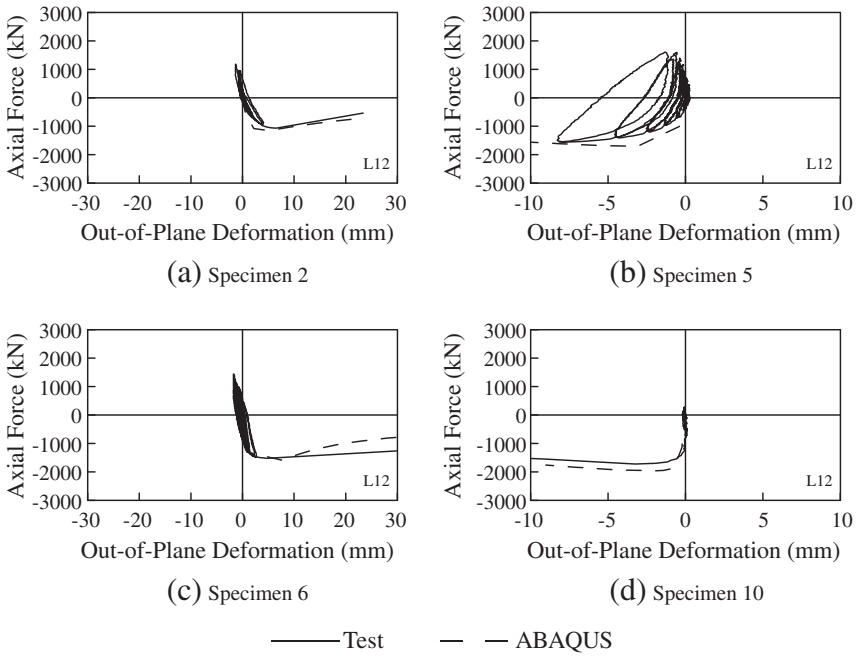

Fig. 12. Comparison between test and finite element analysis results.

4.2. Analytical results

Ultimate compression load, $P_{cr,ABA}$, obtained from finite element analysis, agrees well the test result, $P_{cr,Test}$ (Table 3). The $P_{cr,Test}/P_{cr,ABA}$ ratio was in the ranges of 0.88–1.07. Fig. 12 shows axial compression force versus out-of-plane displacement of the dual gusset plates. The out-of-plane deformation along the gusset length predicted by finite element analysis is close to

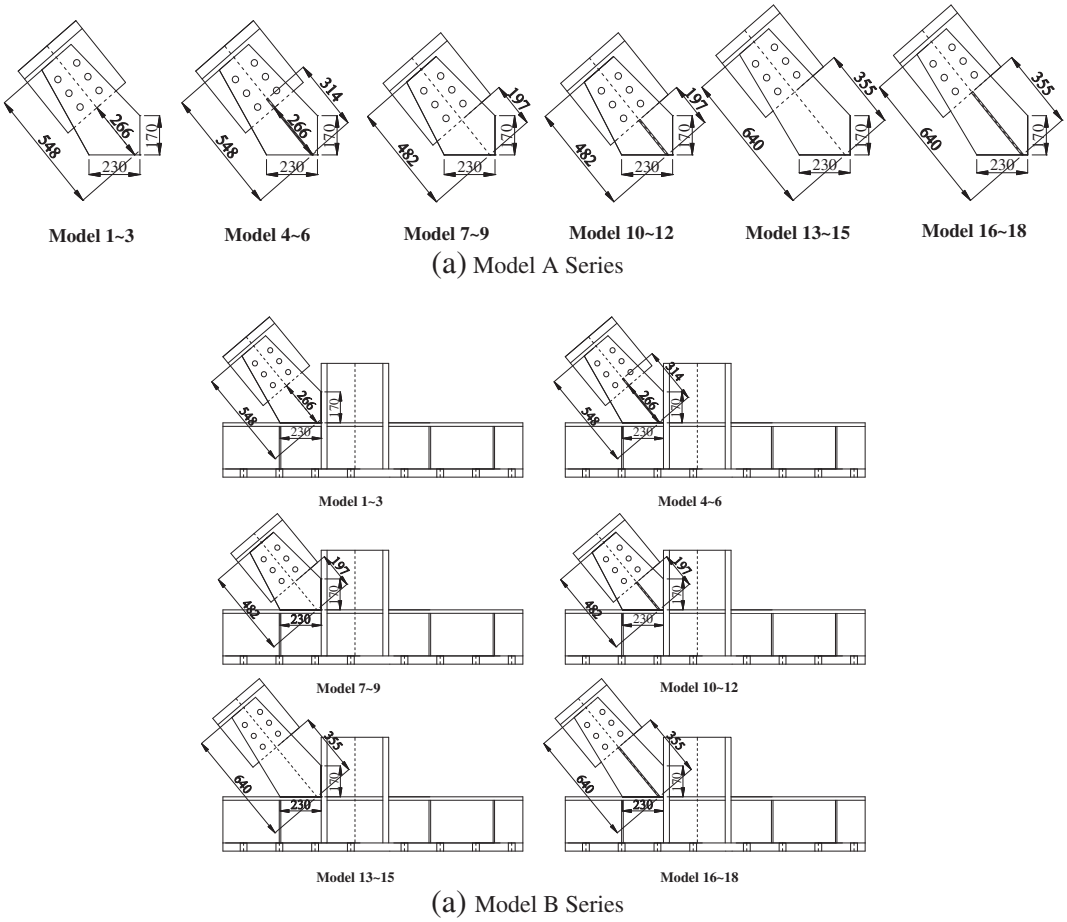

Fig. 13. Finite element models for a parametric study.

Table 4
Compression between finite element analysis and prediction.

Model	t (mm)	b_e (mm)	$P_{cr,\,Th}$ (kN)	$P_{cr,\,GC}$ (kN)	$P_{cr,\,As}$ (kN)	$P_{cr,\,AL}$ (kN)	$P_{cr,\,Ts}$ (kN)	$P_{cr,\,CY}$ (kN)	$P_{cr,\,A}$ (kN)	$P_{cr,\,B}$ (kN)	$\frac{P_{cr,B}}{P_{cr,A}}$	$\frac{P_{cr,A}}{P_{cr,AL}}$	$\frac{P_{cr,B}}{P_{cr,CY}}$
1	8	248	1492	1503	1450	1480	1368	924	1390	1010	0.73	0.94	1.09
2	12	248	2244	2256	2195	2229	2099	1555	2156	1454	0.67	0.97	0.94
3	18	248	3374	3387	3322	3358	3219	2605	3226	2684	0.83	0.96	1.03
4	8	248	1773	1779	1749	1766	1701	1412	1744	1416	0.81	0.99	1.00
5	12	248	2524	2532	2491	2514	2426	2033	2531	2142	0.85	1.0	1.05
6	18	248	3652	3662	3612	3640	3533	3043	3541	2951	0.83	0.97	0.97
7	8	263	1590	1597	1564	1587	1516	1091	1652	1075	0.65	1.04	0.99
8	12	263	2388	2396	2358	2385	2302	1789	2381	1930	0.81	1.0	1.08
9	18	263	3587	3595	3555	3584	3495	2926	3586	2793	0.78	1.0	0.95
10	8	263	1867	1871	1852	1866	1824	1554	1715	1542	0.90	0.92	0.99
11	12	263	2665	2671	2645	2663	2607	2240	2615	2234	0.85	0.98	1.00
12	18	263	3863	3870	3838	3860	3792	3339	3819	3317	0.87	0.99	0.99
13	8	235	1403	1419	1335	1371	1201	748	1007	701	0.70	0.73	0.94
14	12	235	2113	2132	2035	2077	1876	1306	1698	1360	0.80	0.82	1.04
15	18	235	3183	3202	3099	3144	2927	2268	3015	2304	0.76	0.96	1.02
16	8	235	1688	1697	1650	1670	1571	1262	1610	1390	0.86	0.96	1.10
17	12	235	2397	2409	2345	2373	2238	1815	2140	1809	0.85	0.90	1.00
18	18	235	3464	3479	3401	3435	3268	2737	3240	2629	0.81	0.94	0.96

that predicted by the test when ultimate compression load was reached.

4.3. Parametric study

A parametric study was conducted using ABAQUS to investigate the compression behavior and strength of dual-gusset-plate connections. The parameters were gusset size, plate thickness, presence of centerline stiffeners, and gusset plate boundaries. In total, 18 models (Fig. 13(a)) were analyzed; Table 4 lists thickness, t, and Whitmore width, b_e, of a gusset plate. Gusset plate thicknesses were 8, 12, and 18 mm. Two boundary conditions, named Model A and Model B series, were used in the study. The beam and column were not included in the Model A series (Fig. 13(a)); thus, the boundary conditions of dual gusset plates on the beam and column were fixed. The beam and column used in the test setup were included in the Model B series (Fig. 13(b)), such

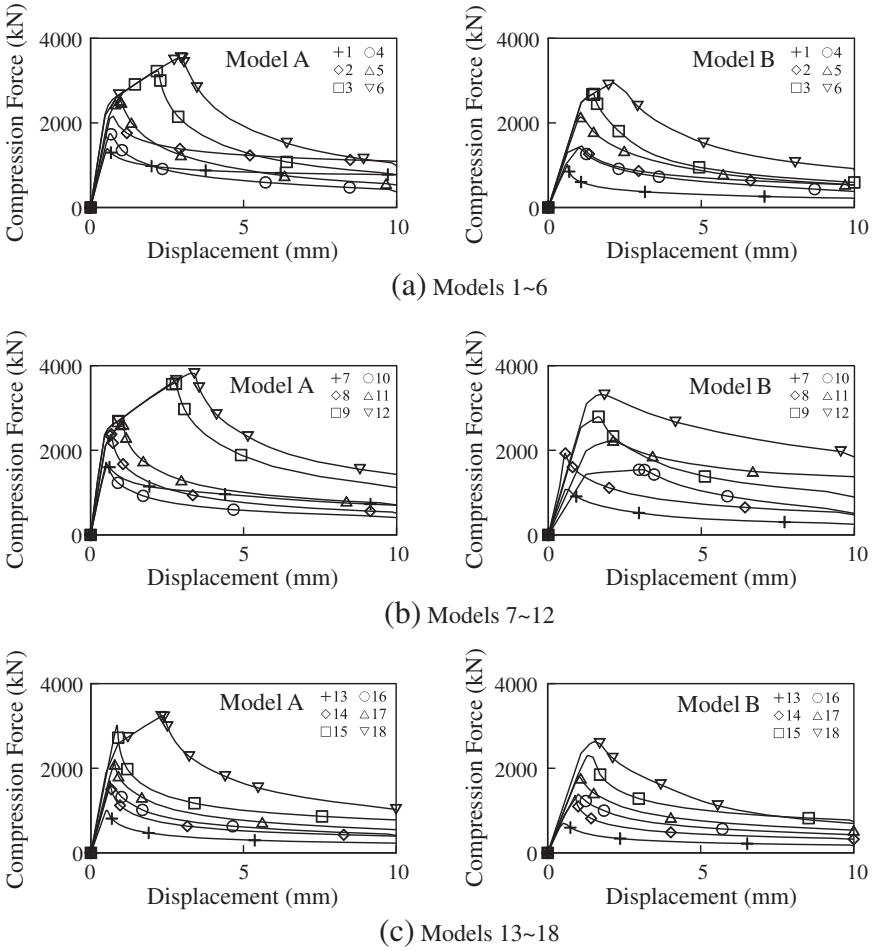

Fig. 14. Axial force versus axial displacement relationship.

that the beam flange could move laterally when dual gusset plates buckled. Ultimate compression loads in both models were used to examine the effects of gusset plate boundaries on ultimate compression load. Axial displacement was applied to the T device to simulate transfer of axial loads from the BRB to the dual gusset plates. Fig. 14 shows axial load versus axial displacement in all models. Generally, by using thick dual gusset plates (18 mm in Models 3, 6, 9, 12, and 18), ultimate compression load increased gradually to a post-yield strength level, and subsequent strength decay due to inelastic buckling occurred at an axial deformation of roughly 3 mm. A long gusset plate (Model 15) did not reach the post-yield strength level without centerline stiffeners.

4.3.1. Gusset plate thickness and size

A roughly linear relationship existed between ultimate compression load and gusset plate thickness in Models 1 to 3, Models 7 to 9, and Models 13 to 15 (Table 4). The symbols, $P_{cr,A}$ and $P_{cr,B}$, represent ultimate compression loads obtained from finite element analyses for Models A and B series, respectively. Moreover, ultimate compression load of the gusset plate increased when gusset length, L_e, decreased.

4.3.2. Centerline stiffeners

When dual gusset plates had centerline stiffeners along both sides, the ultimate compression load of the gusset plate increased significantly, especially for the thin and long gusset plates. In the Model B series, this increase was as high as 2 times when compared to ultimate compression loads, $P_{cr,B}$, of Models 16 and 13 (Table 4). With the same centerline stiffeners, ultimate compression load of the dual gusset plate connection increased as plate thickness increased (Models 10–12 and Models 16–18).

4.3.3. Beam and column

The ultimate compression load of the dual-gusset-plate connection with the beam and column, $P_{cr,B}$, was lower than that with a fixed boundary condition, $P_{cr,A}$. This reduction was as high as 35% (Table 4). Note that the ultimate compression loads predicted by previous studies [8,11,13–16] were close to those predicted by Model A, but not by Model B, because column strip lengths were measured from the Whitmore section to the beam-to-column interface. When the column strip length was extended to the workpoint of the beam and column centerlines, the prediction, $P_{cr,CY}$, was close to the ultimate compression load in the Model B series, $P_{cr,B}$.

5. Conclusions

A single gusset plate connecting the BRB and frame is usually large, requiring many splice plates because the BRB core and gusset plate are in-plane. A dual-gusset-plate connection, sandwiching the BRB core, is proposed as a novel configuration that eliminates the need for splice plates, reduces gusset size, and enhances the stability of gusset plates under compression. The compression behavior of dual-gusset-plate connections was examined via tests and finite element analyses. A parametric study was conducted to study the effects of plate thickness, plate length, presence of centerline stiffeners, and gusset boundaries on ultimate load. Test results of full-scale one-story BRBFs using dual-gusset-plate connections can be found elsewhere [22]. Test and analytical results of dual-gusset-plate connections in compression are summarized as follows:

1. The ultimate compression load of a dual-gusset-plate connection increased as plate thickness increased. By adopting centerline stiffeners, the ultimate compression load increased significantly, especially for the thin and long gusset plates. The beam flange, which was not laterally supported, deformed laterally when the dual-gusset-plate connection was under compression. Thus, predictions based on previous works [8,11,13–16] overestimated the ultimate compression load due to the underestimation of column strip length in Eq. (1). When considering out-of-plane beam deformation, the effective column strip length should be measured from the Whitmore section to the workpoint of the beam and column centerlines. Ultimate compression loads of dual gusset plates determined by tests were reasonably predicted based on the proposed column strip length and a buckling coefficient, K, of 2 in Eq. (1).
2. The finite element analysis program ABAQUS [17] can be used to predict the ultimate compression load and out-of-plane deformation of dual-gusset-plate connections in tests. The parametric study shows that ultimate compression loads of dual gusset plates increased as the plate thickness increased and decreased as column strip length increased. Particularly, a dual-gusset-plate connection reduced the axial load by 10–35% when the beam and column were included in the gusset boundary instead of using a fixed boundary condition.

The authors propose a method to consider the effect of the beam flange deformation on ultimate compression load of the dual-gusset-plate connection by using the effective length of the strut measured from work point to brace end only if the beam flange is free to move. The current practice is applicable to predict ultimate compression load of the single-gusset-plate connection if the beam flange is restrained, not allowed to move laterally. Although the use of the column strip length from work point to brace end can reflect the effect of the beam flange deformation on ultimate compression load of the dual-gusset-plate connection, the effect of the beam depth on ultimate compression load of the gusset needs to be further investigated.

References

[1] Uang CM, Nakashima M. Steel buckling-restrained braced frames. In: Bozorgnia Y, Bertero VV, editors. Earthquake Engineering from Engineering Seismology to Performance-based Engineering (Chapter 16). Boca Raton, FL: CRC Press LLC; 2003. p. 16-1–16-37.
[2] Sabelli R, Mahin SA, Chang C. Seismic demands on steel braced-frame buildings with buckling-restrained braces. Eng Struct 2003;25:655–66.
[3] Prinz GS, Richards PW, Fremming S. Seismic response of buckling-restrained frames with beam splices. 14th world Conference on Earthquake Engineering, Beijing, China; 2008.
[4] Chou C-C, Chen S-Y. Subassemblage tests and finite element analyses of sandwiched buckling-restrained braces. Eng Struct 2010;32:2108–21.
[5] Chou C-C, Liu J-H. Frame and brace action forces on steel corner gusset plate connections in buckling-restrained braced frames. Earthquake Spectra (112410EQS197M, accepted for publication).
[6] AISC. Seismic provisions for structural steel buildings. Chicago, IL: American Institute of Steel Construction; 2005.
[7] Aiken LD, Mahin SA, Uriz P. Large-scale testing of buckling-restrained brace frames. Proceedings, Japan Passive Control Symposium. Japan; 2002.
[8] Tsai K-C, Hsiao B-C, Wang K-J, Weng Y-T, Lin M-L, Lin K-C, et al. Pseudo-dynamic tests of a full scale CFT/BRB frame—Part I: Specimen design, experiment and analysis. Earthquake Eng Struct Dyn 2008;37:1081–98.
[9] Chou C-C, Chen P-J. Compressive behavior of central gusset plate connections for a buckling-restrained braced frame. J Constr Steel Res 2009;65(5):1138–48.
[10] Cheng JJ, Yam CH, Hu SZ. Elastic buckling strength of gusset plate connections. J Struct Eng, ASCE 1994;120(2):538–59.
[11] Thornton WA. Bracing connections for heavy construction. Eng J, AISC 1984: 139–48 Third Quarter.
[12] Whitmore RE. Experimental investigation of stresses in gusset plate. Bulletin No. 16. University of Tennessee: Engineering Experiment Station; 1952.
[13] Gross JL, Cheok G. Experimental study of gusseted connections. Eng J, AISC 1990;27(3):89–97.
[14] Astaneh-Asl A. Seismic behavior and design of gusset plates. Structural Steel Educational Council; 1998.
[15] AISC. Manual of steel construction load and resistance factor design. 3rd edition. Chicago, IL: American Institute of Steel Construction; 2001.
[16] AISC. Design examples. Version 14. Chicago, IL: American Institute of Steel Construction; 2011.
[17] ABAQUS, standard user's manual version 6.3. Pawtucket, RI: Hibbitt, Karlsson & Sorensen, Inc; 2003.
[18] IBC. International Building Code. Falls Church, Virginia: International Code Council; 2000.

[19] Tsai K-C, Lin B-Z. Development of an object-oriented nonlinear static and dynamic 3D structural analysis program. CEER/R92-04. National Taiwan University: Center for Earthquake Engineering Research; 2003.
[20] Sheng N, Yam CH, Iu VP. Analytical investigation and the design of the compressive strength of steel gusset plate connections. J Constr Steel Res 2002;58: 1473–93.
[21] CSA. CAN-CSA-S6-88-Design of highway bridges. Rexdale, Ontario: Canadian Standards Association (CSA); 1988.
[22] Chou C-C, Liu J-H, Pham D-H. Steel buckling-restrained braced frames with single and dual corner gusset connections: seismic tests and analyses. Earthquake Eng Struct Dyn 2011, doi:10.1002/eqe.1176 available on line.